Exploring optical aberrations with two experimental techniques. Applications on Ophthalmic Optics.

Antonio Marzoa Domínguez
Optics and Photonics Research Group, Applied Physics Department, University of Barcelona,

E-mail: amarzodo7.alumnes@ub.edu

Abstract. This work focuses on the general description of two methods for wavefront analysis: wavefront measurement by means of Shack-Hartmann (SH) wavefront sensor and Point-Diffraction Interferometry (PDI); and its potential applications. The basis of each technique is broadly described and a dual experimental set-up configuration is presented and its corresponding results are shown. A general overview and description of geometrical aberrations is carried out, in order to present the mathematical framework that these techniques are based on. The main goal of this work is to experimentally demonstrate the equivalence of this both techniques within the experimental error (i.e. to point out the limit of the equivalence between results obtained with both techniques), and to show if it is possible to design a complete dual set-up which uses both techniques for wavefront characterization. Finally, application of those techniques in the field of Ophthalmic Optics is pointed out through the proposal of different set-ups.

Keywords: Wavefront analysis, Wavefront sensing, Interferometry, Optical Aberrations, Optical Metrology.

1. Introduction: Optical Aberrations

Optical quality assessment of optical systems is a keynote interdisciplinary research topic.
Since the 2nd century BC, people use glass for making lenses in order to enlarge the image of a certain object. For instance, Seneca (4 BC – 65) noticed that a globe of water introduces a magnification when looking through that object one tries to read small letters [1]. Later, in 1276, Franciscan clerk Roger Bacon (1214 – 1292) in his *Opus majus* [2] is the first who talks about that those "globes" of glass (lenses) can be used to correct some vision defects. More precisely, he said that they are a very useful tool for elder people in order to be able to read small letters. Then, around 1600, people discovered and noticed the fact that combining those lenses optical instruments could be made [1]. Thus, during the last 500 years, mankind has worked on improving these instruments for their application in many different scientific and technological areas. Just to mention few of them: Microscopy, Astronomy, medicine, lighting and illumination, photography [3] [4]. Thus, the importance of the quality of this instruments points out as an interesting and relevant topic in order to improve its performance in those areas [5]. Furthermore, the study of the human eye for the detection and correction of its defects and the improvement of its performances is an area of particular and relevant interest itself [5].

It is a well-known result from Geometrical Optics that, knowing the geometrical (curvature radii) and optical (refractive index) parameters of the components that compose an optical system it is possible to determinate the position and the size of the image of an object seen through this system [6]. If the optical system has revolution symmetry and the conditions of paraxial optics are respected, it is possible to obtain a perfect optical representation between pairs of points. These conditions are very restrictive in real optical systems, and then the image starts to present some defects that are known as optical aberrations (or geometrical aberrations). For the reasons pointed

out before, it seems reasonable and interesting to analyze and quantify those aberrations, in order to compensate it and to improve the quality of the optical instrument under test.

2. Theoretical background

As a general idea, geometrical aberration could be defined as the deviation that a wavefront experiments at the exit pupil (ExP) of an optical system respect the ideal wavefront [7]. When the conditions above commented are fitted, the ideal wavefront is spherical which means that there is not aberration and, furthermore, that all the rays that comes from the object point goes to the image point.

If a light ray travels a certain distance s through a homogeneous medium of refractive index n then, the optical path L is defined as follows:

$$L = ns \tag{1}$$

If in its journey the ray passes through different mediums with different values of the refractive index n_i, travelling different distances s_i, then the optical path would be:

$$L = \sum_i n_i s_i \tag{2}$$

The most relevant ray from all of those which travels from the object point is the so-called chief ray (CR). If all the rays that are emerging from the object point are drawn in such a way that all of them present the same optical path of the CR, their tips generate a surface which is called the wavefront. In the case when this surface is spherical and presents its centre of curvature at the position of the paraxial or Gaussian image of the object point, the resulting image is perfect [6]. This essentially means that the optical path travelled by all the rays that emerge from a certain point P and reach the corresponding image point P' is the same. Moreover, if the emerging wavefront deviates from the spherical one (which is also called the reference sphere, RS) then the image is aberrated. This means that rays does not travel the same optical path and its intersection with the paraxial plane is not a point P'. The distance between the intersection points of each ray and the position of the paraxial image is the ray aberration (RA). Thus, the wavefront aberration (WA) corresponding to a certain ray which intercepts the reference sphere at a certain point Q, is defined as the optical path difference between the ray under consideration and the CR. Basic scheme of this definition is shown in Figure 1.

Thus, the WA can be mathematically expressed as:

$$W(x, y) = \tilde{P}P' - P'\tilde{Q} \tag{3}$$

With this result, one can obtain the relationship between ray and wavefront aberrations and, making some mathematical development, it is possible to write the WA as a development of power series [6] [7]:

$$W(x_0, y_0; x, y) = \sum_{j=0}^{\infty} x_0^j \sum_{k=0}^{\infty} y_0^k \sum_{l=0}^{\infty} x^l \sum_{m=0}^{\infty} y^m \, a_{jklm} \tag{4}$$

Where a_{jklm} are the expansion coefficients of the series. This expression is referred to the coordinates at the ExP plane (x_0, y_0) and in the image plane (x, y). Finally, with this mathematical proceed one can compute the WA by means of ray tracing [6] [8].

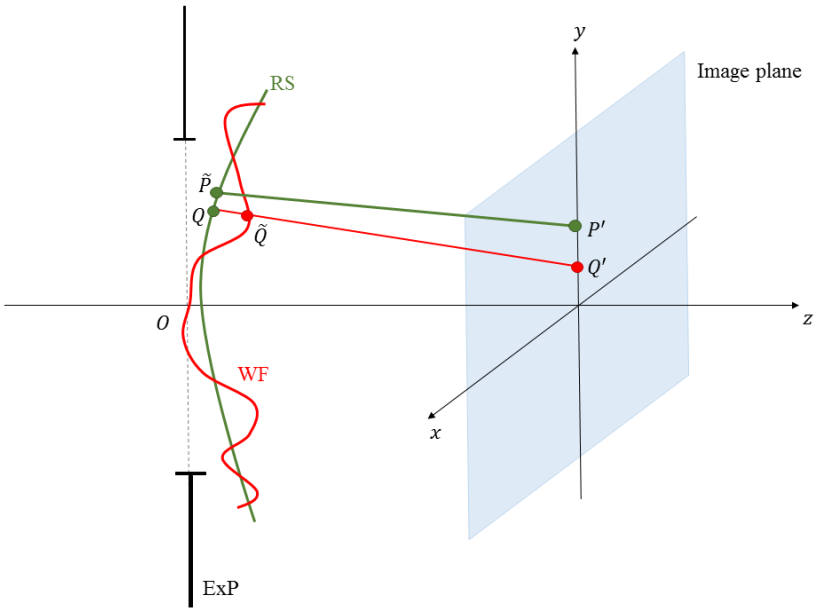

Figure 1. Basic scheme of an aberrated wavefront (which is the actual wavefront, WF) for an on-axis point object. $\tilde{P}$ is the point over the RS refered to the object point P, whereas $\tilde{Q}$ is the point over the WF which corresponds to the ray that intercepts the RS at the point Q.

2.1. Zernike Polynomials

The wavefront aberration of an optical system can be expressed as a function of a complete[1] set of polynomials [7]. There are many sets of polynomials that fits this condition, but there is one broadly used in Optics which was introduced in 1934 by the Nobel Prize Fritz Zernike (1888 – 1966) [9].

Zernike polynomials are orthonormal and continuous over a unit circle. Since the majority of commonly-used optical systems present circular or spherical components and rotationally symmetry, Zernike polynomials in polar coordinates ($x = \rho\cos\theta$, $y = \rho\sin\theta$) are a good choice for describing wavefronts generated by those kind of systems.

As was mentioned before, in general, a function $W(\rho,\theta)$ which describes an arbitrary wavefront in polar coordinates (ρ and θ), can be expressed in terms of a polynomial expansion as follows [10] [11]:

$$W(\rho,\theta) = \sum_{n=0}^{\infty}\sum_{m=0}^{n} C_n^m Z_n^m(\rho,\theta) \tag{5}$$

Where C denotes the Zernike coefficient (also known as amplitude, Zernike term or "weight") which corresponds to a certain polynomial term $Z(\rho,\theta)$. Using polar coordinates, these polynomials are given by a complex combination as follows:

$$Z_n^m(\rho,\theta) \pm Z_n^{-m}(\rho,\theta) = R_n^m(\rho)e^{\pm im\theta} \tag{6}$$

Which directly leads to the formulae:

$$Z_n^m(\rho,\theta) = R_n^m(\rho)\cos(m\theta) \qquad m \geq 0 \tag{7.1}$$
$$Z_n^m(\rho,\theta) = R_n^{-m}\sin(m\theta) \qquad m < 0 \tag{7.2}$$

[1] The term "complete" implies that any reasonably well-behaved function can be expanded as a series of functions of the set.

Where the radial function $R_n^m(\rho)$ is given by the following expression [9] [10]:

$$R_n^m(\rho) = \sum_{l=0}^{(n-m)/2} \frac{(-1)^l (n-l)!}{l!\left[\frac{1}{2}(n+m)-l\right]!\left[\frac{1}{2}(n-m)-l\right]!} \rho^{n-2l} \tag{8}$$

Since these polynomials are orthonormal in the unit circle, the normalization is chosen in such a way the condition $R_n^{\pm m}(\rho = 1) = 1$ is satisfied for any value of n and m. Thus,

$$N_n^m = \left[\frac{2(n+1)}{1+\delta_{m0}}\right]^{1/2} \tag{9}$$

Is the normalization constant; where δ_{m0} is the so-called Kronecker delta ($\delta_{m0} = 0$ for $m \neq 0$). At that point, it is important to comment that two different nomenclatures are used in Zernike expansion for wavefront analysis. When the N_n^m constant is included inside the C_n^m coefficient, the expansion is known as Zernike Peak-to-Valley (PV) polynomials (also known as Wyant nomenclature), whereas when N_n^m is explicitly included in the expression, the corresponding name is Zernike RMS polynomials or Noll's expansion [12]. This comment is necessary since the commercial software used in this work to obtain Zernike expansion from experimental data permits the use of both developments. In our study, Wyant nomenclature is used.

In order to simplify the notation of those polynomials we can use Noll's sequential indices [12] in order to pass from $Z_n^m(\rho, \theta)$ to $Z_j(\rho, \theta)$. The basic rule for doing that is that the polynomial which presents an even value of m obtains an even index j, and the other-way-round for the odd m indices. Whitin a given n, lower values of m obtain lower j indices. For instance, the polynomial Z_2^{-2} corresponds to Z_5, whereas Z_2^2 corresponds to the polynomial Z_6, according to Noll's notation.

In order to show the relation of Zernike polynomials with classical geometrical aberrations, Table 1 show few of those polynomials and its corresponding expression. A graphical representation is presented in Figure 2.

Table 1. Most known and relevant orthonormal Zernike circle polynomials and its corresponding aberrations.

j	n	m	N_n^m	Zernike polynomial	Z_j	Aberration name
1	0	0	1	1	Z_1	Piston
2	1	1	2	$\rho\cos\theta$	Z_2	Tilt in X direction
3	1	-1	2	$\rho\sin\theta$	Z_3	Tilt in Y direction
4	2	0	$\sqrt{3}$	$2\rho^2 - 1$	Z_4	Defocus
5	2	-2	$\sqrt{6}$	$\rho^2\sin(2\theta)$	Z_5	Astigmatism at 45º
6	2	2	$\sqrt{6}$	$\rho^2\cos(2\theta)$	Z_6	Astigmatism at 0º
7	3	-1	$\sqrt{8}$	$(3\rho^3 - 2\rho)\sin\theta$	Z_7	Coma at 90º
8	3	1	$\sqrt{8}$	$(3\rho^3 - 2\rho)\cos\theta$	Z_8	Coma at 0º
11	4	0	$\sqrt{5}$	$6\rho^4 - 6\rho^2 + 1$	Z_{11}	Primary spherical aberration

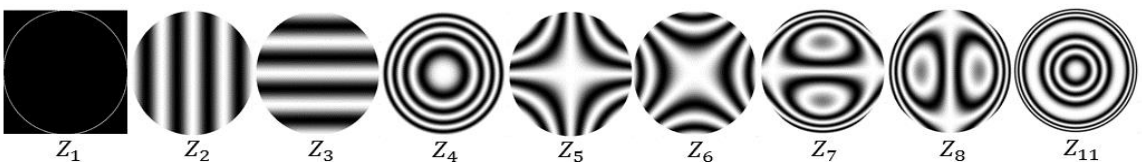

Figure 2. Pictorial representation of the wavefronts (i.e. phase maps) corresponding to aberrations presented in Table 1.

Finally, a common metric of wavefront flatness is the RMS error or wavefront error σ, which is defined in terms of the Zernike coefficients as follows [10]:

$$\sigma = \left(\sum_{j=4}^{N} C_j^2 \right)^{\frac{1}{2}} \tag{10}$$

Where the first few terms, which represents the pseudo-aberrations of piston and tilts are ignored.

3. Shack-Hartmann wavefront sensor

At the beginning of 20th Century, people from the Astrophysical Institute of Postdam reported that the optics of their famous Great Refractor Telescope (an 80 cm refracting telescope) presented inadequate quality. German astrophysicist Johannes Hartmann (1865 – 1936) proposed to set a screen with a series of holes in it, at the aperture of the telescope. With this configuration, Hartmann was able to test the optical quality of the telescope by using the spot diagram generated with this mask.

In late 1960s, the Optical Science Center (OSC) at the University of Arizona by the US Air Force, pointed out a technical problem: Earth's atmosphere limits the image quality and exposure time in some astronomical observations from terrestrial observatories. Dr. Roland Shack (Chicago, Illinois, USA, 15th January 1927) found the solution: he took the classical Hartmann and replaced the array of holes used at that time by an array of lenses [13]. Then, the Shack-Hartmann (SH) (sometimes called Hartmann-Shack) wavefront sensor device was born.

Nowadays, a SH sensor basically consists on a microlens array and a CCD camera. The wavefront which is tended to be measured is divided by the microlens array in such a way that each light division is brought to a particular location in the focal plane of the array. If the wavefront is aberrated, these spots shift from the regularly spaced ideal spot pattern produced by a plane wavefront (see Figure 3). These displacements provide information on the local slope of the wavefront over each microlens, and then the WA can be reconstructed using an indicated software.

Although originally designed to be used in correction atmosphere turbulence in optical Astronomy [14], during the last past two decades SH sensors have successfully been used in other fields such as the analysis and compensation of ocular aberrations [15], or the generation of optical tweezers [16] and the correction of its aberrations [17]. For those reasons, a SH wavefront sensor seems to be a powerful tool in order to analyze the quality of optical instruments.

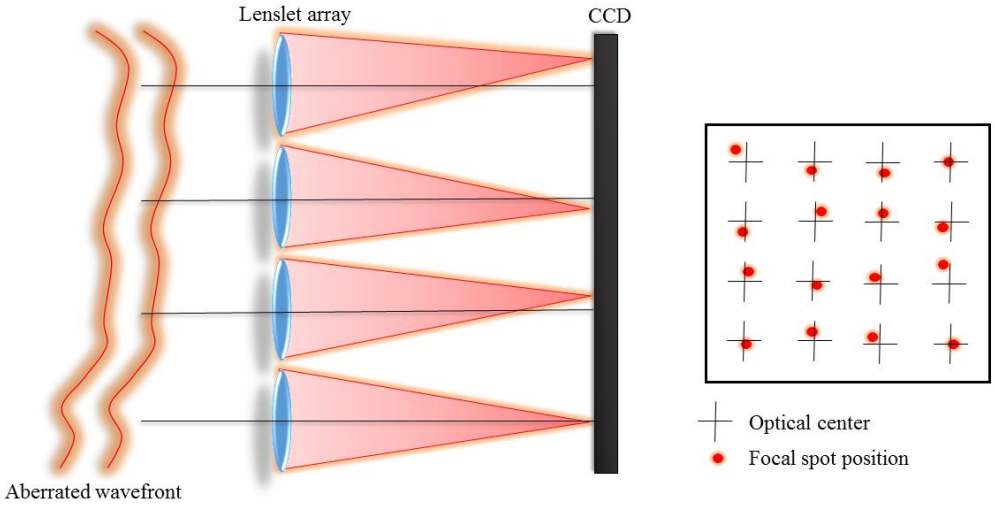

Figure 3. Schematic of a SH wavefront sensor working when an aberrated wavefront reaches the microlens array.

4. Point-Diffraction Interferometer

In 1933, a new kind of single interferometer for measuring phase variations across a wavefront was introduced [18]. Furthermore, in early 1970s, R. N. Smartt, from University of Massachusetts, reintroduced the instrument and set its potential applications [19]. This instrument is the Point-Diffraction Interferometer (PDI), which is a simple common-path interferometer used to directly measure optical path differences. A PDI basically consists on a semitransparent plate with a clear pinhole, as shown in Figure 4.

When a light beam reaches the plate, a spherical reference wave is produced by diffraction at the clear pinhole while the rest of the beam passes through the plate without any change in phase. If the size of the pinhole and the transmittance of the plate are chosen in such a way that both beams have similar amplitude, well contrasted fringes will be observed in any plane placed after the plate. Figure 4 illustrates the basis of this technique.

The basic principle of the PDI can be derived from spatial-filtering theory: the sum of the complex amplitudes of the wave being examined and a plane reference wave gives as its Fourier transform the amplitude image from the original wave plus a delta function.

In recent years, this instrument has been taking some relevant interest in the field of Ophthalmic Optics for the characterization of progressive lenses [20]. Since progressive lenses generate complex wavefronts [21] and PDI is capable to analyse them, this technique seems to be a powerful and relevant tool in the study of noisy beams such the ones generated by biological samples. In this direction, relevant implementations has been reported in the analysis of fish lenses [22].

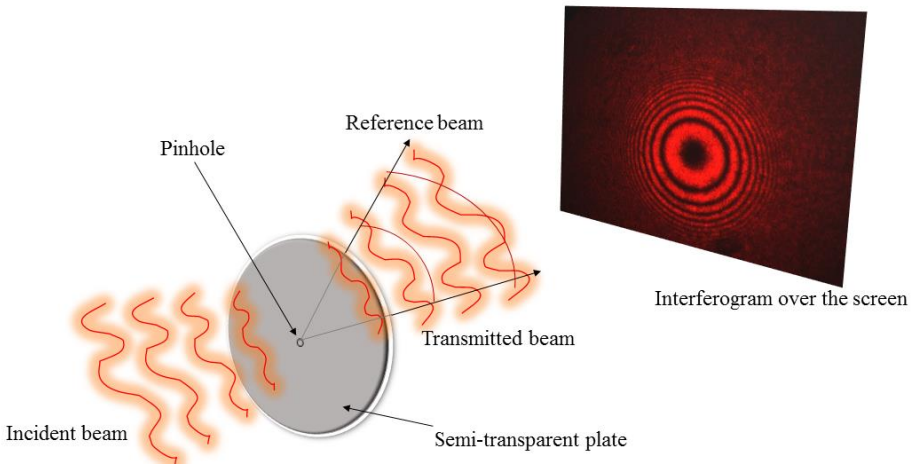

Figure 4. Basic principle of PDI.

5. Experimental set-up

Our goal is to see the equivalence of results between both techniques. Thus, in order to do that, maintaining the same conditions of measurements using both techniques is necessary. For this reason, a dual set-up should be designed taking into account the differences of measurement configurations of both techniques.

In order to perform the experiments, the best measuring configuration is to send plane waves to the system under test. This essentially is translated into put a collimating lens in the optical bench which will send a collimating beam to the optical system. In our set-up, an achromatic doublet of 500 mm of focal length is used.

The SH sensor works with collimated light (i.e. with plane wavefronts). Thus, a conjugation lens is required in order to bring the aberrated wavefront to the SH entrance pupil. Furthermore, this system needs to provide a total magnification in such a way all the measuring area enters in the

sensors surfaces, otherwise we will be "cutting" the wavefront and therefore losing some information.
According to Abbe – Rayleigh image formation theory [23] [24], all the aberrating and diffracting effects of the optical system are considered at its ExP. Thus, this conjugation lens has another function: to bring the image of the ExP to the microlenses array plane. Considering this requirements, a photographic objective with 50 mm of focal length was chosen as a conjugating system.

Other limitation of the experiment is that the PDI works with coherent light. For this reason a He-Ne laser ($\lambda = 633$ nm) was used in all the experiments.

The lens under test used in this study was a biconvex lens with a focal length of 200 mm of focal length. The semitransparent plate of the PDI was made by coating a glass substrate with Cr. The optical density was 2.5 and the pinhole diameter was 15 μm. This plate was mounted over a xyz support.
Finally, the SH device used in this work was a HASO32TM from the Imagine Optics Company. The lenslet array consists on 32x32 microlenses and a 512x512 pixels CCD sensor of 5x5 mm area.

Considering all those requirements, the set-up shown in Figure 6 was mounted in an optical bench. When measurements are done, first the SH configuration (see Figure 6 a)) is used and then, the wavefront sensor is removed and replaced by a simple CCD camera and the PDI is placed near the focus region of the system under test (see Figure 6 b)).

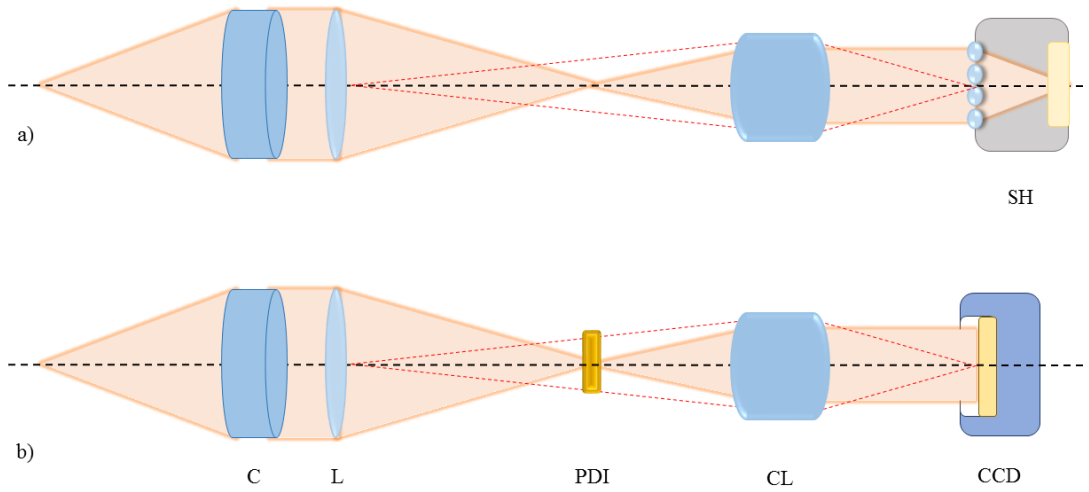

Figure 6. Scheme of the set-up designed and used in the laboratory. Light travels from left to right, and C represents the collimating lens, L the optical system to be analysed (which in this case was a single biconvex lens), and CL represents the conjugation lens. a) is the configuration for measurements using SH wavefront sensor and b) for PDI analysis. Red-dotted lines show the formation of the image of the wavefront of the ExP over the measurement plane.

A software for computing Zernike coefficients is supported by the manufacturer for the SH device used in this study. For the computation of those coefficients from the interferogram the *Atmosfringe*® software [25] was used.

6. Results

Since we are interested in observing high-order aberrations, tilts and also defocus aberrations were always excluded. Moreover, since the system under test is a conventional biconvex lens, just the coefficients up to 11^{th} order were considered, because higher orders are null for this kind of systems. Otherwise, including more coefficients in the development will imply adjusting noise.

For the measurement carried out with the biconvex lens under test, results shown in Table 2 were obtained. The maximum difference between results for each coefficient is about $\lambda/30$. A pictorial representation of the wavefront is shown in Figure 7, and a visual inspection shows that both techniques provide quite similar results. This image was obtained implementing equation (5) in a MATLAB® code. For each data set, the σ and PV values were computed.

Table 2. Value of the Zernike coefficients measured with both techniques and absolute value of its differences. Those results are graphically represented in Figure 7 c).

Zernike term	Value (in λ units) for SH measurement	Value (in λ units) for PDI measurement	Difference (in λ units)
5	0.2309	0.2463	0.0154
6	-0.2189	-0.2292	0.0103
7	0.1496	0.1369	0.0127
8	-0.0971	-0.0683	0.0288
11	-0.0833	-0.0907	0.0074

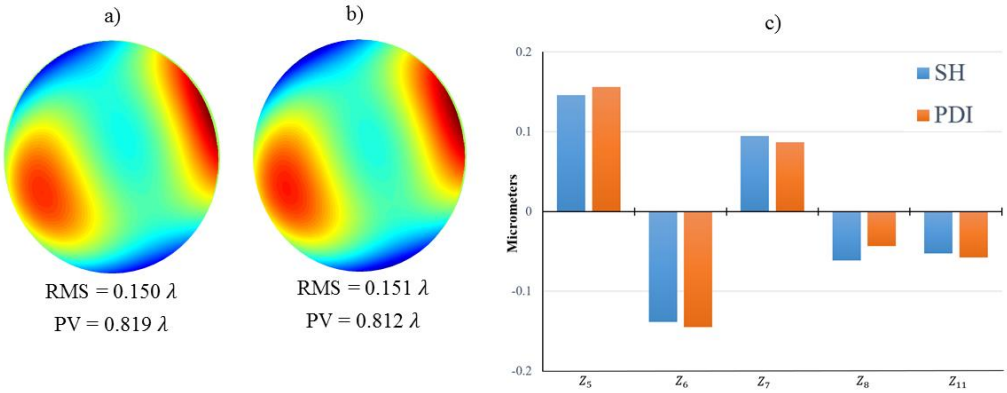

Figure 7. WA computed in MATLAB® with SH data (a)) and with PDI results (b)). RMS (σ) and PV values for each measurement are also included in the figure. There are not notifiable or relevant differences between both reconstructions. Tilts and defocus were always excluded. c) is a graphical representation of values of Table 2.

7. Discussion

Equivalence of results between SH and PDI was experimentally proved with a difference in the RMS between both techniques of 0.001 λ (0.007 μm) and a maximum difference between measured Zernike coefficients of 0.03 λ (0.02 μm). This equivalence was previously reported by Bueno et al. [26] for the case of phase plates obtaining a maximum difference in the RMS of $\lambda/10$. As far as we know, no-one has presented or reported this equivalence in the case of real imaging systems as it was done in this work.

As was briefly commented in each method section, both techniques used in this work are operationally different, and each one presents advantages and disadvantages respect the other.

On the one hand, PDI is a very simple technique due to the fact that it is composed by one simple optical element. The interference pattern provided by PDI can be easily interpreted as the phase aberration of the wave, plus some small amount of defocus and tilt in case the pinhole is not correctly placed at focus. This technique permits the direct visualization of the constant phase fringes. However, the computation of the WA requires post-processing of the images from manual tracking dark fringes using [25], with the accuracy limitations that a manual procedure implies.

On the other hand, SH wavefront sensor is a well-known, widely and commonly used device in ocular, astronomical and optical testing applications. Unlike the PDI, the analysis to obtain WA can be done in real time, which allows easy experimental alignment. Moreover, this sensor does not precise monochromatic light for measuring, but presents the drawback that details smaller

than microlenses size are not resolved or detected. Development of a dual compact set-up combining both techniques seems to be able to provide a robust design.

8. Conclusions

We have demonstrated the equivalence of two different and complementary techniques (PDI and SH sensor) for measuring the WA of imaging optical systems such as single lenses under the same experimental conditions. Despite the noticeable differences between both techniques, results provide the same information within the experimental error. In different applications, the combined use of both techniques, could offer the optimum solution, by merging high resolution from the PDI with the robustness of SH.

Since there are commercial devices for characterization of progressive addition lenses based on SH sensors [27] and the PDI has been shown as a potential technique for characterizing those systems [22] we are interested on the development of an integrated set-up which includes both techniques. Some experiments were carried out at the end of this study in that direction, and what was observed is that this kind of spectacle lenses need a mapping system for the measurements.

Another interesting and potential application of the results of this work in the field of Ophthalmic Optics is related to intraocular lens (IOL) characterization. The optical characterization of IOLs provides objective and quantitative information that is essential to fully understand their performance as an implant that replaces the crystalline lens in the human visual system after cataract surgery [28]. Additionally, it can be used to predict the performance of the new IOL designs. In that sense, we are interested in the development of another dual set-up in an optical bench for the characterization of IOLs using both SH and PDI. Preliminarily works [29] presented interesting designs for characterizing these systems. Moreover, it has to be pointed out that the characterization of multifocal intraocular lenses (MIOLs) can not be done in terms of SH wavefront sensor [30], and since these systems provide non-continuous patterns it is also impossible to analyze them using a PDI. Thus, we are limited to the analysis of monofocal IOLs with the techniques presented in this work.

Currently we are developing a system for characterizing IOLs with both a SH and a PDI. In order to do that, a model of the eye is being settled in an optical bench and the conditions of ISO 11979-2:2014 are took into account.

Acknowledgments

This work was supported by the “Agencia Estatal de Investigación” (AEI) and the Fondo Europeo de Desarrollo Regional” (FEDER), under Project FIS2016-77319-C2-2-R of the Spanish “Ministerio de Economía, Industria y Competitividad”. I am indebted to my advisor, Prof. Dr. Santiago Vallmitjana for his help, advising, supervision and encouragement throughout the course of this work. Also I want to thanks Dr. Salvador Bosch for his interesting comments and computational help and the rest of people of the Optics and Photonics Group for being nice with me during the development of this work. Finally, I also want to thank Dr. María S. Millán and Dr. Mertixell Vilaseca from UPC for the material that they give to me for the IOL’s characterization experiments that we are currently carrying on.

References

[1] Darrigol O, 2012 *A History of Optics: From Greek Antiquity to the Nineteenth Century* (Oxford University Press)
[2] Juvells I and Moliné R M, 2005 Representacions de personatges amb lents a l’art dels Països Catalans dels segles XIV I XV *Revista de Física* (29) 16-21
[3] Hecht E, 2000 *Optics* (Madrid: Addison Wesley Iberoamericana)
[4] Johnson B K, 1960 *Optics and Optical Intruments* (New York, Dover Publications Inc.)
[5] Vallmitjana S, 2009 25 anys d’Òptica. Què podem veure que no vèiem abans? *Revista de Física* **4** (7) 32-40

[6] Smith W J, 2000 *Modern optical engineering* (New York: McGraw-Hill)
[7] Born M and Wolf E, 2001 *Principles of Optics* (Cambridge University Press)
[8] Abbad F, 1973 *Estudios de criterios de optimización para el cálculo automático de sistemas ópticos* (Universitat de Barcelona, PhD)
[9] Zernike F, 1934 Beugungstheorie des Schneidenverfahrens und Seiner Verbesserten Form, der Phasenkontrastmethode *Physica* **1** (8) 689-704
[10] Lakshminarayanan V and Fleck A, 2011 Zernike polynomials: a guide *Journal of Modern Optics* **58** (7) 545-561
[11] Mahajan V N, 2011 *Aberration Theory Made Simple* (Bellingham: SPIE Press)
[12] Noll R J, 1976 Zernike polynomials and atmospheric turbulence *J. Opt. Soc. Am.* **66** (3) 207-2011
[13] Platt B C, 2001 History and principles of Shack-Hartmann wavefront sensing, *J. Refract. Surg.* 17 573-577
[14] Duffner R W and Fugate R Q, 2009 *The Adaptive Optics Revolution: A History* (University of New Mexico Press)
[15] Liang J, Grimm B, Goelz S and Bille J F, 1994 Objective measurement of wave aberrations of the human eye with the use of a Hartmann-Shack wave-front sensor *J. Opt. Soc. Am.* **11** (7) 1949-1957
[16] Rodrigo P J, Eriksen R L, Daria V R and Glückstad J, 2003 Shack-Hartmann multiple-beam optical tweezers *Opt. Express* **11** (3) 208-214
[17] López-Quesada C, Andilla J and Martín-Badosa E, 2009 Correction of aberration in holographic optical tweezers using Shack-Hartmann sensor *App. Optics* **48** (6) 1084-1090
[18] Linnik W P, 1933 A Simple Interferometer for the Investigation of Optical Systems *C. R. Acad. Sci, URSS* 5 (210)
[19] Smartt R N and Steel W H, 1975 Theory and Application of Point-Diffraction Interferometers *Japan J. Appl. Phys.* **14** (1) 351-355
[20] Acosta E, Chamadoira S and Blendowske R, 2006 Modified point diffraction interferometer for inspection and evaluation of ophthalmic components *J. Opt. Soc. Am.* **23** (3) 632-637
[21] Chamadoira S, 2011 *Interferómetro de difracción por orificio, IDO, para la inspección y caracterización de lentes progresivas* (Universidae de Santiago de Compostela, PhD. Thesis)
[22] Vallmitjana S, Ricart I, Bosch S, Gargallo A and Acosta E, 2015 Point diffraction interferometry to measure local curvatures and caustics of noisy wave fronts: Application for determining optical properties of fish lenses *J. Eur. Opt. Soc.-Rapid* **10** 15010
[23] Abbe E, 1873 Beiträge zur Theorie des Mikroskops un der Mikroskopischen wahrnehmung *Archiv für Mikroskopische Anatomie* **9** 413-468
[24] Rayleigh L, 1896 On the theory of optical images, with special references to the microscope *Phil. Mag.* **46** (5), 167
[25] Atmosfringe: http://www.atmossoftware.it/AtmosFringe.html
[26] Bueno J M, Acosta E, Schwarz C and Artal P, 2009 Wavefront measurements of phase plates combining a point-diffraction interferometer and a Hartmann-Shack sensor
[27] Huang C, Raasch T W, Yi A Y, Sheedy J E, Andre B and Bullimore M A, 2012 Comparison of Three Techniques in Measuring Progressive Addition Lenses *Optometry and Vision Science* **89** (11) 1564-1573
[28] Güell J L, Morral M, Kook D and Kohnen T, 2010 Phakik intraocular lenses – Part 1: Historical overview, current models, selection critwria, and surgical techniques *Journal of Cataract & Refractive Surgery* **36** (11) 1976-1993
[29] Alba-Bueno F, Millán M S and Vega F, 2017 Optical Characterization of Intraocular Lenses *Opt. Pura Apl.* **50** (1) 63-73
[30] Castignoles F, Lepine T, Chavel P and Cohen G, 2011 Shack-Hartmann multiple spot with diffractive lenses *Optics Letters* **36** (8) 1422-1424